ELSEVIER

Journal of Quantitative Spectroscopy & Radiative Transfer 100 (2006) 457–469

Journal of Quantitative Spectroscopy & Radiative Transfer

www.elsevier.com/locate/jqsrt

Effect of ice crystal shape and effective size on snow bidirectional reflectance

Yu Xie[a], Ping Yang[a,*], Bo-Cai Gao[b], George W. Kattawar[c], Michael I. Mishchenko[d]

[a]*Department of Atmospheric Sciences, Texas A&M University, College Station, TX 77843, USA*
[b]*Remote sensing Division, Code 7232, Naval Research Laboratory, Washington, DC 20375, USA*
[c]*Department of Physics, Texas A&M University, College Station, TX 77843, USA*
[d]*NASA Goddard Institute for Space Studies, 2880 Broadway, New York, NY 10025, USA*

Abstract

We tested the applicability of three rigorous radiative transfer computational approaches, namely, the discrete ordinates radiative transfer (DISORT) method, the adding–doubling approach, and an efficient computational technique based on Ambartsumian's nonlinear integral equation for computing the bidirectional reflectance of a semi-infinite layer. It was found that each of these three models, in a combination with the truncation of the forward peak of the bulk scattering phase functions of ice particles, can be used to simulate the bidirectional reflectance of a semi-infinite snow layer with appropriate accuracy. Furthermore, we investigate the sensitivity of the bidirectional reflectance of a homogeneous and optically infinite snow layer to ice crystal habit and effective particle size. It is shown that the bidirectional reflectance is not sensitive to the particle effective size in the visible spectrum. The sensitivity of the bidirectional reflectance in the near-infrared spectrum to the particle effective size increases with the increase of the incident wavelength. The sensitivity of the bidirectional reflectance to the effective particle size and shape is attributed fundamentally to the sensitivity of the single-scattering properties to particle size and shape. For a specific ice crystal habit, the truncated phase function used in the radiative transfer computations is not sensitive to particle effective size. Thus, the single-scattering albedo is primarily responsible for the sensitivity of the bidirectional reflectance to particle size, particularly, at a near-infrared wavelength.

1. Introduction

Snow substantially reflects the solar radiation at visible wavelengths; additionally, snow also significantly absorbs near-infrared radiation. Because of its pronounced effect on the radiation budget of the earth–atmosphere system, snow plays a significant role in the terrestrial climate system and its evolution. Satellite-based remote sensing of snow often requires the use of forward radiative transfer models to simulate the bidirectional reflectances of snow sheets. In most previous modeling efforts, "equivalent spheres" were commonly assumed, although realistic snow particles are almost exclusively nonspherical ice crystals with

*Corresponding author. Tel.: +1 979 845 4923.
E-mail address: pyang@ariel.met.tamu.edu (P. Yang).

0022-4073/$ - see front matter © 2005 Elsevier Ltd. All rights reserved.
doi:10.1016/j.jqsrt.2005.11.056

various complicated morphologies such as aggregates and polycrystals. For example, Wiscombe and Warren [1] simulated snow albedo as a function of wavelength using a two-stream radiative transfer code and assuming the spherical equivalence for snow particles. Dozier [2] carried out extensive modeling simulations of snow reflectance properties using the discrete ordinates radiative transfer (DISORT) code developed by Stamnes et al. [3] in the two-stream mode. The former assumed "equivalent ice spheres" to implement a snow masking algorithm involved in the analysis of the Landsat TM data. Grenfell [4] compared the observed snow albedo with the theoretical results from the Lorenz–Mie theory. Painter and Dozier [5] simulated in situ hemispherical–directional snow reflectance spectra using DISORT with 20 streams, who also assumed "equivalent ice spheres" in their analysis. Most recently, Kokhanovsky et al. [6,7] compared in situ measurements of snow reflectance with calculations from Mishchenko et al.'s model [8] based on the representation of snow grains as random-fractal particles. To properly simulate the bidirectional reflectance of snow, a rigorous radiative transfer computational model in conjunction with reliable single-scattering properties of snow particles is indispensable.

The intent of the present study is first to validate the applicability of three existing radiative transfer codes, namely, DISORT [3], the adding–doubling model developed by de Hann et al. [9], and an efficient computational model for a semi-infinite medium developed by Mishchenko et al. [8]. Because the bulk scattering phase function of ice crystals normally has a forward peak that is associated with the diffraction of the incident light for large size parameters, two truncation techniques, namely, the δ-M method developed by Wiscombe [10] and the δ-fit method developed by Hu et al. [11], are used to truncate the forward peak in this study. It was found that a combination of the fast Radiative Transfer Equation (RTE) method developed by Mishchenko et al. [8] and the δ-fit method [11] for phase function truncations is most appropriate for the numerical calculation of snow reflectance. With this RTE model, the bidirectional reflectance is computed for an optically infinite and homogeneous snow layer consisting of nonspherical ice crystals, by assuming five habits (or shapes) for snow particles. The sensitivity of the bidirectional reflectances to different particle sizes and shapes is investigated; particularly, the effects of two basic scattering parameters, the single-scattering albedo and phase function, on the bidirectional reflectance of snow are also investigated.

This paper is organized as follows. The bidirectional reflectance of a snow sheet is defined in Section 2. In Section 3, the theoretical basis of three rigorous radiative transfer models involved in the present study are concisely recaptured, where the truncation of the forward peak of the phase function is also briefly described. The numerical results and discussions are presented in Section 4. Finally, the conclusions of this study are given in Section 5.

2. Bidirectional reflectance

Bidirectional reflectance is defined as the ratio of the reflected intensity along a direction toward the detector to the incident intensity [12], which implies a comparison of the reflected intensity from a surface with that from an absolutely white Lambertian surface. If the incident source of radiation is the sun, the bidirectional reflectance can be defined as follows:

$$R(\mu,\phi;\mu_0,\phi_0)=\frac{I(\mu,\phi)}{\mu_0 F/\pi}=\frac{\pi I(\mu,\phi)}{\mu_0 F}, \tag{1}$$

where $\mu=\cos\theta$ and $\mu_0=\cos\theta_0$ in which θ_0 and θ are the solar and viewing zenith angles, respectively; ϕ_0 and ϕ are the azimuthal angles of the sun and the detector, respectively; F is the direct solar irradiance at the top of the atmosphere; and $I(\mu,\phi)$ is the specific intensity emerging from the top of the atmosphere toward the detector. Note that the atmospheric absorption due to various gases is not accounted for in this study.

Bidirectional reflectance of a surface is intrinsically associated with the reflectance, absorptance and roughness of the surface. Therefore, it provides valuable information on the optical characteristics of the surface.

To compute the bidirectional reflectance of snow, in this study we assume a plane–parallel layer with an optically semi-infinite medium composed of randomly oriented ice particles.

3. Comparison of computational techniques

3.1. DISORT with δ-fit truncation

3.1.1. DISORT

The DISORT model developed by Stamnes et al. [3] is based on the discrete ordinates method pioneered by Chandrasekhar [13]. In this method, the specific intensity I is solved on the basis of the classical radiative transfer equation for a plane–parallel atmosphere, given by

$$\mu\frac{\mathrm{d}I(\tau,\mu,\phi)}{\mathrm{d}\tau} = I(\tau,\mu,\phi) - \frac{\tilde{\omega}}{4\pi}\int_0^{2\pi}\mathrm{d}\phi'\int_{-1}^{1} I(\tau,\mu',\phi')P(\mu,\varphi;\mu',\phi')\,\mathrm{d}\mu' - \frac{\tilde{\omega}}{4\pi}FP(\mu,\phi;\mu',\phi')\mathrm{e}^{-\tau/\mu_0} + (1-\tilde{\omega})B[T(\tau)], \tag{2}$$

where τ is the optical depth, $\tilde{\omega}$ is the single scattering albedo, F is the direct solar irradiance, and P is the phase function. Any application of the classical radiative transfer equation is based on an implicit assumption that scattering particles are located in each other's far-field zones [14]. However, particulate surfaces in nature are often composed of closely packed particles [15,16]. Preliminary analyses of the extent to which the classical radiative transfer equation can be applied to such closely packed scattering media have been reported in the literature [e.g., 17,18].

In the framework of the DISORT model, the specific intensity is expanded in a Fourier series as follows:

$$I(\tau,\mu,\phi) = \sum_{m=0}^{N} I^m(\tau,\mu)\cos m(\phi_0-\phi). \tag{3}$$

By expanding the phase function in Eq. (2) and replacing the integral by Gaussian quadrature, each I^m coefficient can be solved for independently in the form of the summation of all the homogeneous solutions and the particular solutions for the multiple-scattered radiation associated with the incident radiation and thermal emission as follows:

$$I^m(\tau,\mu_i) = \sum_j L_j^m\varphi_j^m(\mu_i)\mathrm{e}^{-k_j^m\tau} + Z^m(\mu_i)\mathrm{e}^{-\tau/\mu_0}, \quad i=-n,\ldots,n. \tag{4}$$

The DISORT is applicable to an atmosphere with various layers of arbitrary values of optical thickness, single-scattering albedo, and phase function. Extensive efforts have been carried out to validate the applicability and accuracy of this radiative transfer computational model. The technical details of the DISORT are not recapitulated here since they have been reported in the literature [3].

3.1.2. DISORT with δ-fit truncation

The scattering phase function in DISORT is specified in terms of its Legendre polynomial expansion coefficients. For a phase function with a strong forward peak, thousands of Legendre expansion terms are required. To use a practical number of expansion terms, which means less computer CPU time, the truncation of the forward peak is required. The DISORT computational package contains the δ-M truncation scheme [10]. In this study, we use the δ-fit truncation scheme [11] that is an extension and enhancement of the δ-M scheme. However, different from the δ-M truncation, the δ-fit technique provides the coefficients of Legendre expansion by solving the following equations:

$$\frac{\partial\varepsilon}{\partial c_l} = 0, \quad l=0,1,2,\ldots,N, \tag{5}$$

where ε is the relative difference between actual phase function and truncated phase function. C_l, $l=0,1,2,\ldots,N$ are the coefficients of the Legendre polynomial expansion of the truncated phase function. It is evident from Eq. (5) that the δ-fit technique minimizes the errors associated with the truncation. In this study, we also apply this truncation method to computations based on the adding–doubling method and the unique method developed by Mishchenko et al. [8] for a semi-infinite medium.

3.2. Adding–doubling method

The adding–doubling method for solving the RTE was introduced by van de Hulst [19]. The adding–doubling computational program used in this study is that developed by de Haan et al. [9] that fully accounts for polarization which is a sine qua non for the transfer of radiation. In practice, the doubling method may start with a thin layer with known single-scattering albedo and phase matrix, although Kattawar and Plass [20] showed that this initialization scheme has some disadvantages and suggested a more appropriate approach. Consider combining two parallel layers, one placed on top of the other. Let R_1 and T_1 be the reflection and transmission functions, respectively, for the first layer; whereas R_2 and T_2 are those for the second layer. The bidirectional reflectance and transmission functions of the combined layer are given by employing the adding equations (Eqs. (19)–(25) in Ref. [9]) using R_1, T_1, R_2 and T_2. The reflection and transmission function of a layer with known single-scattering properties but arbitrary optical thickness can be calculated by adding thin layers until the desired optical thickness is reached. The doubling method is a special case of the adding method when the conjoined layers may have the same optical properties, i.e., optical thickness, single-scattering albedo, and phase function.

To reduce the number of integrations in the adding scheme, a Fourier expansion is used in the computational code developed by de Haan et al. [9]. For each Fourier component, a set of azimuth-independent adding equations is derived. The supermatrices are employed to treat the combinations of integrations and matrix multiplications as single matrix products.

Similar to DISORT, the adding–doubling method is also a rigorous method for radiation transfer calculations. One of the advantages of this method is that it is quite effective for computing the reflection or transmission function of a system composed of various vertically inhomogeneous layers.

3.3. Mishchenko et al.'s method

A radiative transfer computational package developed by Mishchenko et al. [8] is quite efficient for computing the bidirectional reflectance of a semi-infinite homogeneous particulate medium. This technique is based on the fact that the bidirectional reflectance can be expanded in a Fourier series as follows:

$$R(\mu,\mu_0,\phi) = R^0(\mu,\mu_0) + 2\sum_{m=1}^{m_{\max}} R^m(\mu,\mu_0)\cos m\phi. \tag{8}$$

The coefficients R^m in Eq. (8) can be determined directly by solving Ambarzumian's nonlinear integral equation [21,22].

Unlike the DISORT and adding–doubling computational programs, the computational technique developed by Mishchenko et al. [8] is restricted to homogeneous semi-infinite scattering layers. However, the advantage of the latter is that the computation of the internal radiation field is avoided, and the efficiency in numerical computation is significant.

3.4. Comparison

Fig. 1 shows the comparison of the performance of the aforementioned three RT computational models. Canonical simulations are carried out with an optical thickness of 2000, single-scattering albedo of 1, and the Henyey–Greenstein (H–G) phase function, with a g of 0.75. The H–G function can be given in the form

$$P(\cos\Theta) = \frac{1-g^2}{(1+g^2-2g\cos\Theta)^{3/2}} = \sum_{l=0}^{N}(2l+1)g^l P_l(\cos\Theta). \tag{9}$$

Evidently, the Legendre expansion coefficients of the H–G function can be exactly obtained, provided the asymmetry factor is given. For this analytical phase function, hundreds of Legendre expansion coefficients in DISORT are needed to give convergent results. Fig. 1 shows the DISORT with an 8-term expansion of the phase function based on the δ-fit method essentially converges to the correct solution with several hundred expansion terms. From the comparison of the results from DISORT with δ-fit (dotted line in Fig. 1) and δ-M

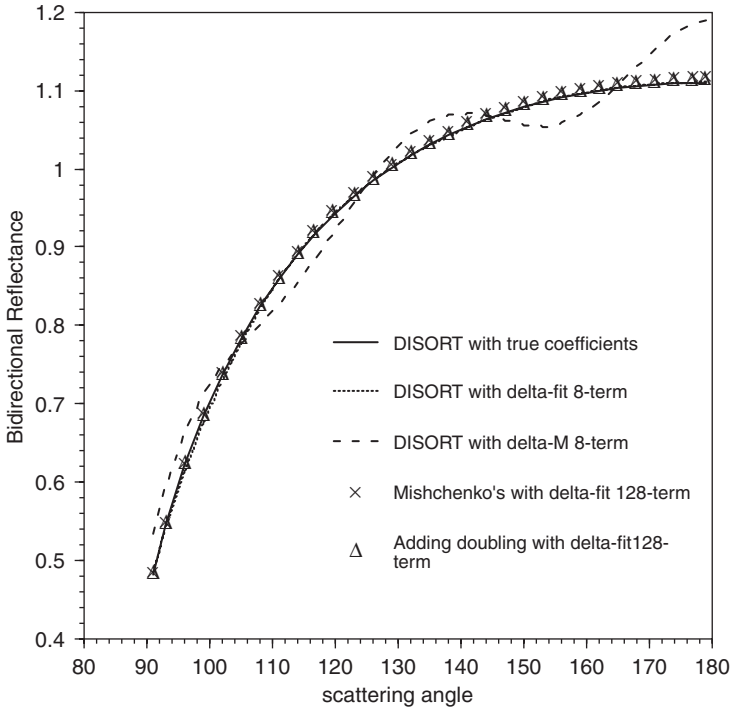

Fig. 1. Comparison of bidirectional reflectances from DISORT with true coefficients, δ-fit and δ-M truncation. Comparison of bidirectional reflectances from DISROT, Mishchenko's code and adding–doubling code.

(dashed line) truncation methods, it is evident that the δ-fit truncation scheme is more accurate when the same number of expansion terms are used. Thus, the δ-fit truncation scheme is used in both Mishchenko et al.'s method and the adding–doubling code in this study. To achieve high accuracy, 128 expansion terms are considered in the δ-fit truncation coefficients. Evidently, the aforementioned three radiative transfer models agree well with each other. However, Mishchenko et al.'s method [8] is especially suitable for a case with a semi-infinite optical thickness because of its computational efficiency. Thus, in this study a combination of the fast Mishchenko et al.'s radiative transfer method and the δ-fit expansion with 128 terms is utilized.

4. Computation and discussion

Five ice particle habits, including aggregates, bullet rosettes, hexagonal solids, hollow columns, and hexagonal plates, are considered in this study. Ice particles are assumed to be randomly oriented. A snow layer is assumed to be homogeneous and optically semi-infinite. The database of single-scattering properties for each particle shape is developed by an improved geometric optics method [23], with 6 wavelengths ranging from 0.4 to 2.2 μm and particle maximum dimensions from 2 to 10,000 μm. Detailed information on the particle geometry and database of the single-scattering properties of ice crystals can be found in Refs. [23–25]. For a given size distribution of ice crystals, the effective size, De, is defined following Foot [26] as follows:

$$De = \frac{3}{2}\frac{\int V(D)n(D)\,\mathrm{d}D}{\int A(D)n(D)\,\mathrm{d}D}, \tag{10}$$

where n indicates the number concentration of ice crystals, D is the characteristic size (normally, the maximum dimension for practical applications) of an ice crystal, and V and A are the volume and projected area of an ice crystal. In this study, we assume a gamma distribution [27] for the population of ice crystals.

Figs. 2 and 3 show the bidirectional reflectance of snow as a function of particle effective size at the wavelengths of 0.4, 0.6, 0.8, 1.2, 1.7 and 2.2 μm for two incident-view configurations. The incident solar zenith

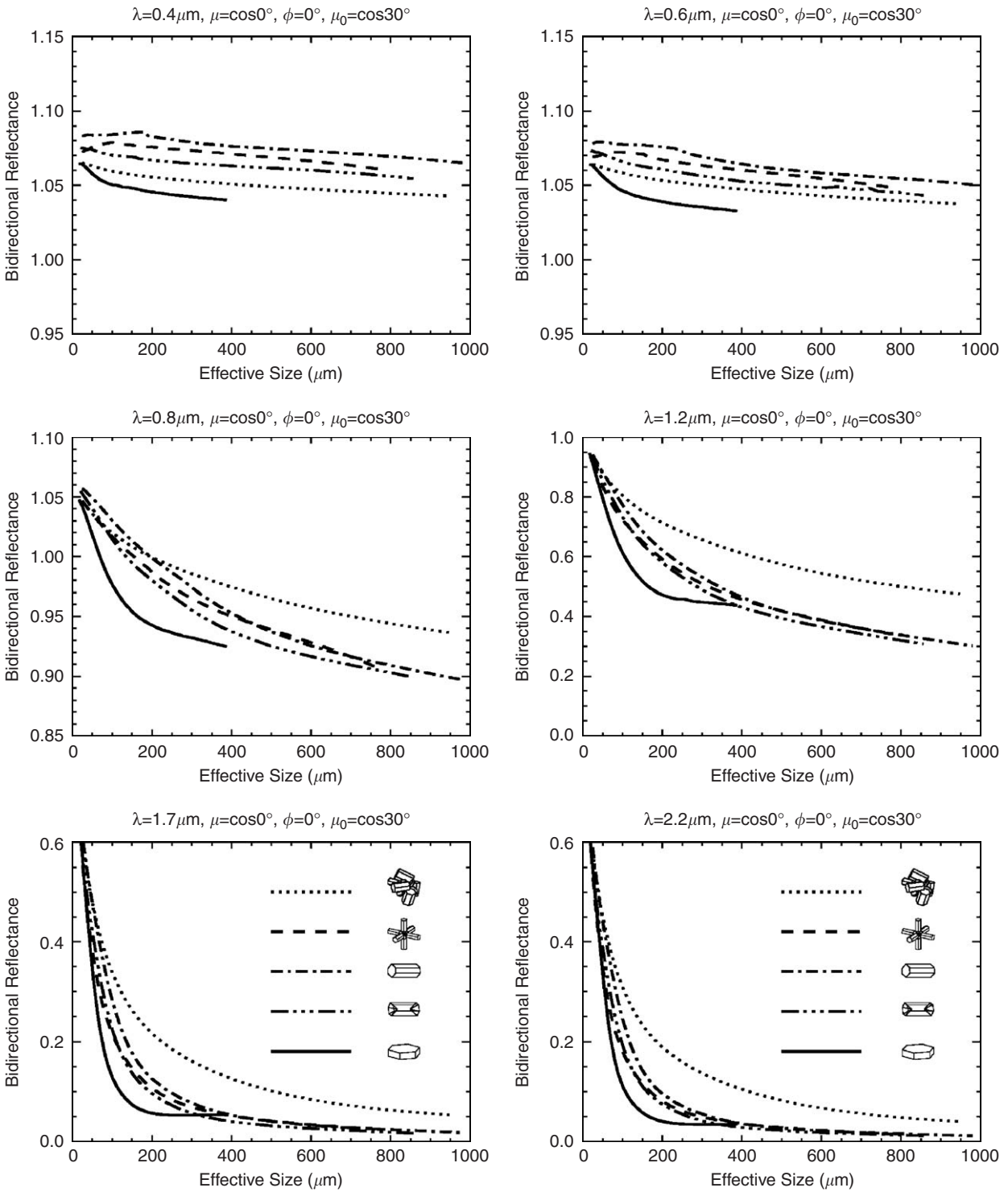

Fig. 2. Bidirectional reflectance versus effective size. The wavelengths for each panel are 0.4, 0.6, 0.8, 1.2, 1.7, and 2.2 μm. Zenith angle, incident solar zenith angle, and relative azimuthal angle are 0°, 30° and 0°, respectively.

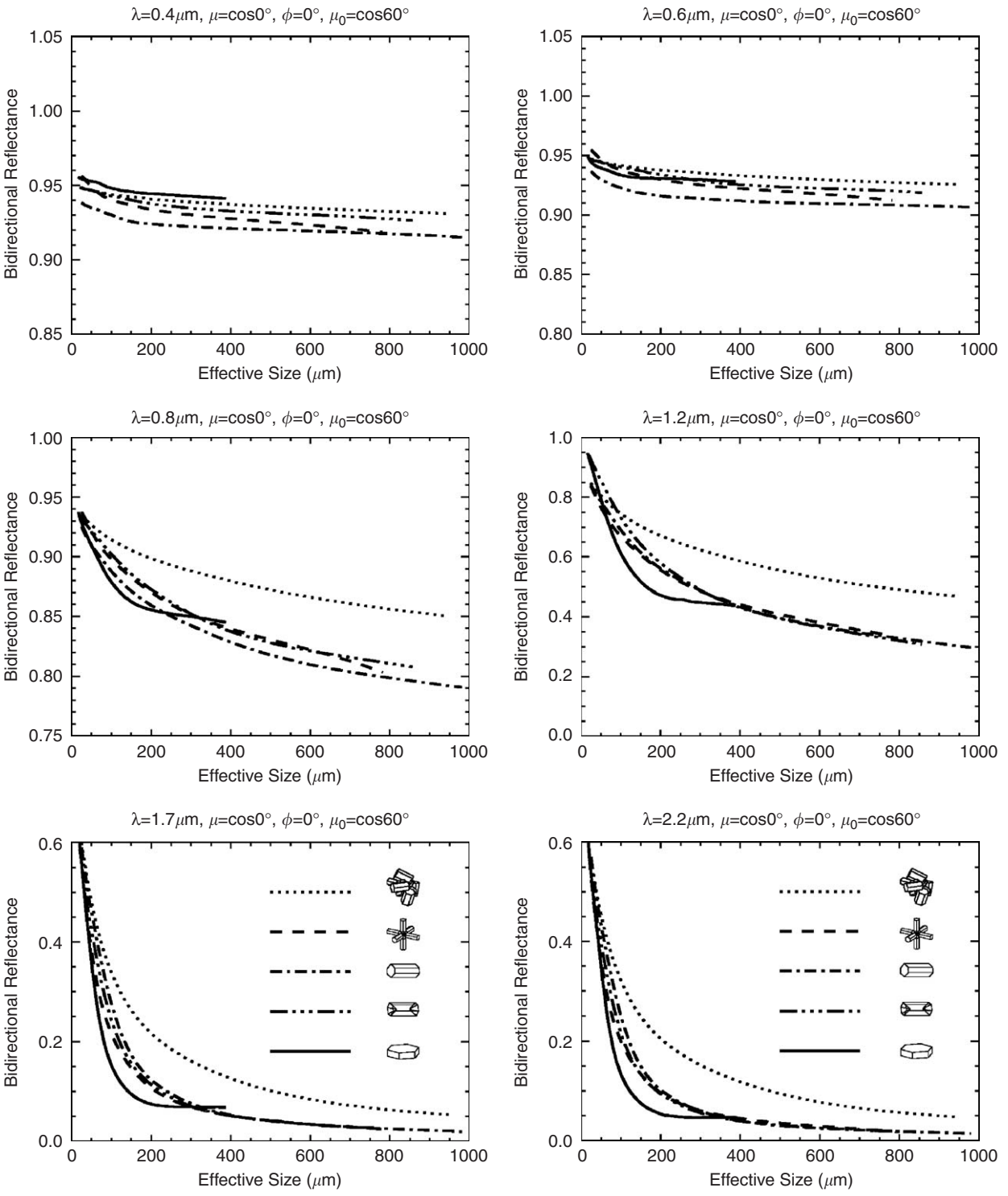

Fig. 3. Bidirectional reflectance versus effective size. The wavelengths for each panel are 0.4, 0.6, 0.8, 1.2, 1.7, and 2.2 μm. Zenith angle, incident solar zenith angle, and relative azimuthal angle are 0°, 60° and 0°, respectively.

angles used in the computations are 30° and 60° for Figs. 2 and 3, respectively. The observing zenith angle and relative azimuthal angle are 0° in both of the cases, that is, the observation of the bidirectional reflectance is at the nadir. The aspect ratio of ice plates [24] results in a limitation on its effective size. Specifically, the effective size increases little with the increase of the maximum dimension because the aspect ratio (i.e., the ratio of the dimension of particle cross section to the particle length) increases and plates become relatively thinner in terms of their aspect ratios. Therefore, the bidirectional reflectance of ice plates shown in Figs. 2 and 3 is available only for an effective size less than 400 μm. The numerical results for other particle shapes, including aggregates, bullet rosettes, hexagonal solids and hollow columns, are given with effective sizes up to 1000 μm.

Evidently, the variation of the bidirectional reflectance with particle effective size becomes more pronounced with an increase in wavelength from 0.4 to 2.2 μm. The bidirectional reflectance in the visible region (the upper two panels in Figs. 2 and 3) is close to 1 and slightly varies with the effective size. However, in the near-infrared region (the middle two and lower two panels), especially when the wavelength is longer than 1.2 μm, the values of bidirectional reflectance decrease with a large gradient, as the effective size increases. The slope of the variation of the bidirectional reflectance for small particles (effective sizes smaller than 400 μm) is negative. For larger particles, the slope of the curves tends to 0 with increasing wavelength. Therefore, the smallest particles have the maximum value of bidirectional reflectance, while the larger particles have minimum value. The numerical differences between the maximum and minimum values in the same panel in Figs. 2 and 3 become larger with the increase of wavelength from 0.4 to 2.2 μm. Moreover, for the same particle size, the values of bidirectional reflectance decrease from the first panel to the last one. For instance, the maximum values change from approximately 1.05 at $\lambda = 0.4\,\mu m$ to values around 0.5 at $\lambda = 2.5\,\mu m$. The minimum values are from approximately 1.05 to 0.0. It is also obvious that the bidirectional reflectance for any certain effective size decreases as the incident solar zenith angle increases from 30° to 60°. The decreasing rate decreases across the spectral region from the visible to the near-infrared.

The sensitivity of the bidirectional reflectances to the five particle shapes is also illustrated in Figs. 2 and 3. An interesting point is that with increasing wavelength, (i.e. moving from the first panel to the last) the variation rate of the bidirectional reflectance for each of the five ice particle habits has a certain trend. The overall trend is that bidirectional reflectance decreases with increasing wavelength for all the ice crystal shapes. However, the bidirectional reflectance decreases more slowly for aggregates than for the other ice crystal shapes. The reflectance associated with plates show significant variations. The trends for the other shapes can be seen with a close examination of Figs. 2 and 3. The sensitivity of the bidirectional reflectances at the near-infrared wavelengths to particle habit is evident.

It is well known that the sensitivity of bidirectional reflectance is related to optical depth, single-scattering albedo, and phase function. The optical depth involved in this study is assumed to be infinite. Therefore, the sensitivity of bidirectional reflectance to the particle size and shape are essentially attributed to the sensitivity of the single-scattering albedo and phase function to the particle size and shape.

Fig. 4 shows the single-scattering albedo with the variation of effective size in the visible and near-infrared regions. In the visible region (the upper two panels in Fig. 4), the single-scattering albedo is not sensitive to effective size and is close to 1 for all the particle shapes. In the near-infrared region (the middle two and lower two panels), the single-scattering albedo decreases as the wavelength increases. Compared with the case shown in Fig. 4, the sensitivity of bidirectional reflectance to effective size shown in Figs. 2 and 3 is strongly related to the single-scattering albedo.

For light scattering by large ice crystals with smooth planar faces such as the cases for hexagonal plates and columns, the scattering phase function can be expressed in the form of

$$P(\theta) = 2f_\delta \delta(\mu - 1) + (1 - f_\delta)\tilde{P}(\theta), \tag{11}$$

where $\mu = \cos\theta$, δ is the Dirac delta function, and the factor f_δ is associated with the delta-transmission of the incident rays through two parallel faces of the scattering particle [28,29]. Note that the phase function P in Eq. (11) is normalized if $\tilde{P}(\theta)$ is normalized. As the sizes of ice crystals (on the order of several tens to hundreds microns, and even up to thousands microns) are much larger than the visible and near-infrared wavelengths, a strong forward peak corresponding to the diffraction of the incident light is associated with $\tilde{P}(\theta)$. In rigorous

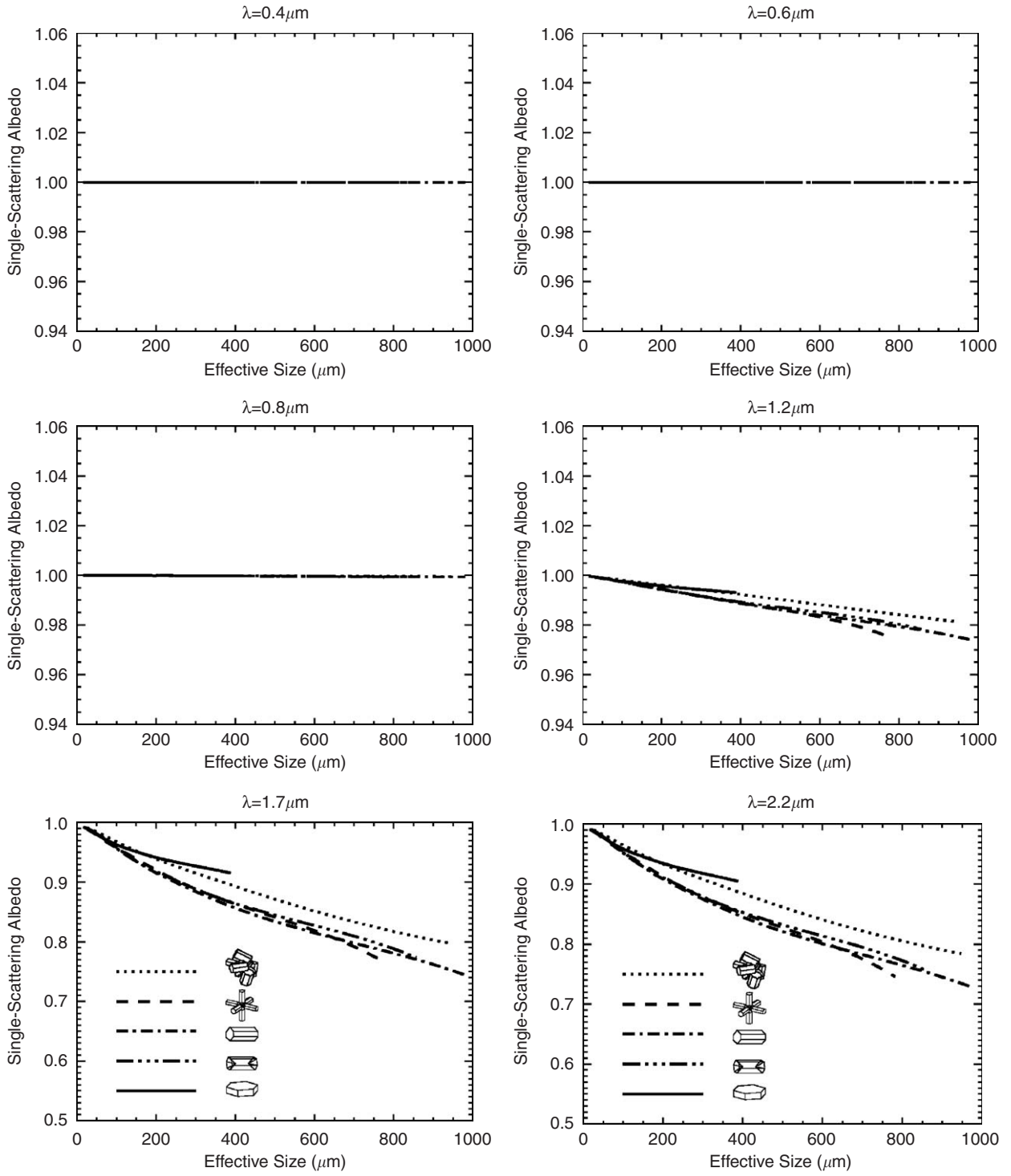

Fig. 4. Single-scattering albedo versus effective size. The wavelengths for each panel are 0.4, 0.6, 0.8, 1.2, 1.7, and 2.2 μm, respectively.

radiative transfer codes, the phase function is normally required to be expanded in terms of Legendre polynomials. The strong forward peak of $\tilde{P}(\theta)$ requires thousands of terms in the Legendre expansion of the phase function if accurate results are expected, leading to substantial computational efforts. To economize

numerical computations in radiative transfer simulations, a common practice is to truncate the forward peak. Let the percentage of the scattered energy associated with the truncated peak be f. Then, the phase function can be approximated as follows:

$$\tilde{P}(\theta) \approx 2f\delta(\mu-1) + (1-f)\tilde{P}'(\theta) \tag{12}$$

or,

$$P(\theta) \approx 2(f_\delta + f - f_\delta f)\delta(\mu-1) + (1-f_\delta)(1-f)\tilde{P}'(\theta). \tag{13}$$

$\tilde{P}'(\theta)$ is the truncated phase function used in the radiative transfer computation. In this study, we use the δ-fit method developed by Hu et al. [11] to derive both $\tilde{P}'(\theta)$ and f from $\tilde{P}(\theta)$. With the truncation of the phase function, other single-scattering parameters (the single-scattering albedo for this study) need to be adjusted on the basis of the similarity principle [29,30].

Fig. 5 shows the truncated phase function $\tilde{P}'(\theta)$ for 5 ice crystal habits as a function of the scattering angle at the wavelengths of 0.4, 0.8 and 2.2 μm. Three effective sizes, 50, 200 and 800 μm are used for aggregates, bullet rosettes, hexagonal solids, and hollow columns whereas effective sizes of 50, 200 and 400 μm are used for plates. Note that for aggregates, surface roughness is accounted for in the computation of the single-scattering properties [25]. Evidently, phase functions are not highly sensitive to the effective size. As the size parameters associated with light scattering by ice crystals are in the geometric optics regime, the side and backscattering feature is essentially from the contribution of the externally reflected rays and the transmitted rays undergoing various orders of internal reflection. At a nonabsorbing wavelength, the phase function in side and backscattering directions are independent of particle size although in the forward direction the diffraction is the dominant contribution and it is dependent on particle size, which is the case for the phase functions at a wavelength of 0.4. The slight dependence of the phase function on the effective size is due to different aspect ratios for particles when the size distribution of ice crystals is considered. For example, for columns, the aspect ratio used in this study is [24]

$$a = \begin{cases} -8.479 + 1.002L - 0.00234L^2, & L \leqslant 200\,\mu\text{m}, \\ 11.3L^{0.414}, & L > 200\,\mu\text{m}, \end{cases} \tag{14}$$

where a is the semi-width of the cross section of a hexagonal column whereas L is length of the particle.

As a snow layer in the present simulation is assumed as a semi-infinite layer, the sensitivity of the bidirectional reflection function is a function of the phase function and the single-scattering albedo. It is evident from Fig. 5 that the phase functions for the three different effective sizes are quit similar at a wavelength of 0.4 μm, a wavelength where the single-scattering albedo is close to 1. Therefore, for a visible wavelength, the bidirectional reflectance of snow is not sensitive to the effective size, as is shown in Figs. 2 and 3. At a near-infrared wavelength, the phase function shows little sensitivity to the effective size, as is evident from Fig. 5. However, the corresponding albedo decreases with effective size, as is shown in Fig. 4. Therefore, the bidirectional reflectance is sensitive to particle size.

5. Conclusions

We investigated the sensitivity of the bidirectional reflectance of a semi-infinite snow layer to the effective particle size and the shapes of ice crystals. Five ice crystal habits (aggregates, bullet rosettes, hexagonal solids, hollow columns, and plates) are assumed for the geometries of ice crystals. The single-scattering properties of these particles were computed from an improved geometric optics method. Furthermore, we investigated the applicability of three radiative transfer codes for a semi-infinite medium. Based on the comparison of the results from the three radiative transfer code, the code developed by Mishchenko et al. [8] in a combination with the δ-fit method for the truncation of the forward peak of the phase function was used in the present simulation because of the computational efficiency of this code.

It is found that the bidirectional reflectance of snow depends slightly on the effective size at visible wavelengths, whereas strong sensitivity of the bidirectional reflectance to particle size is noticed at the near-infrared wavelengths. It is shown that the truncated phase functions used in the radiative transfer

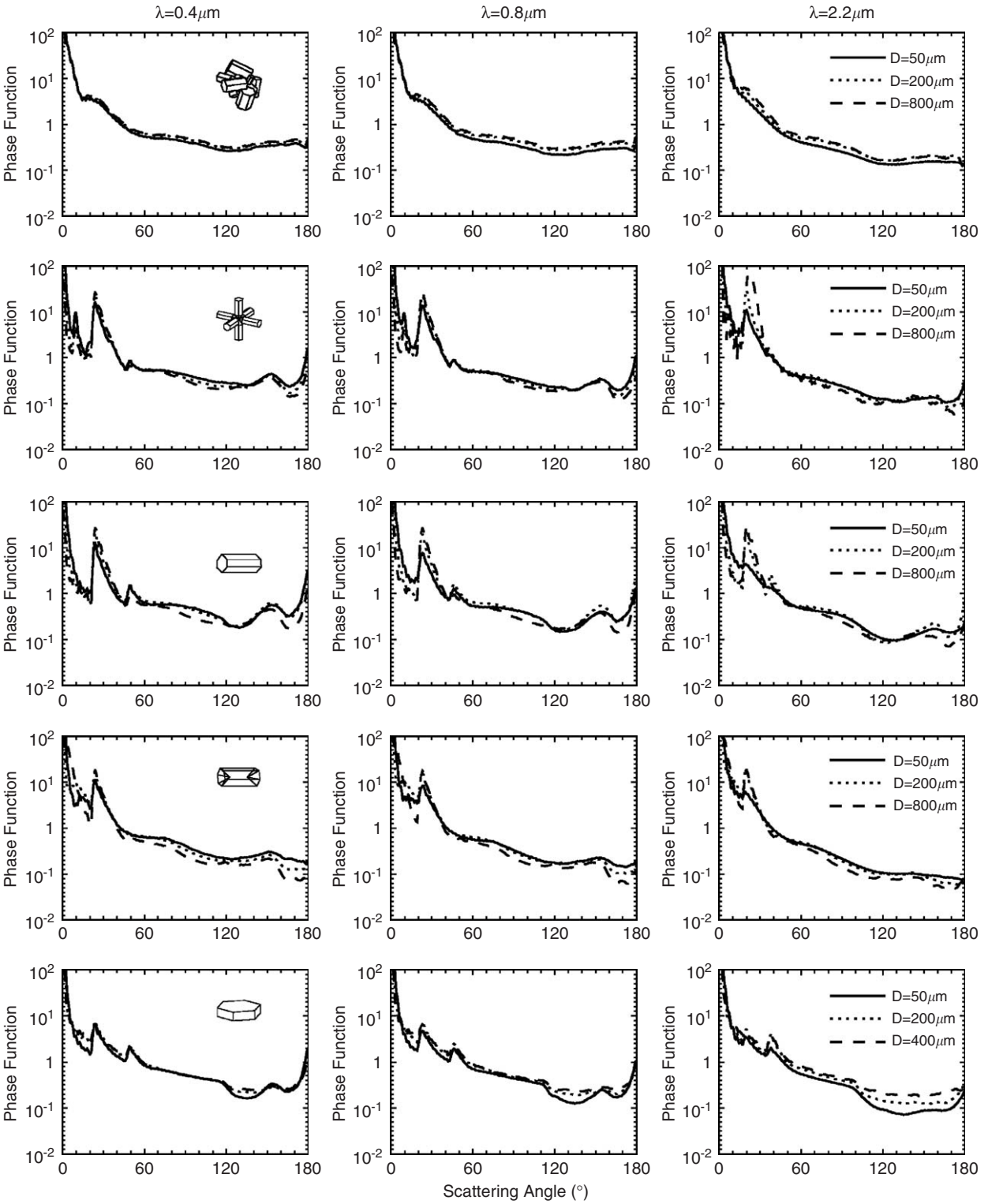

Fig. 5. The phase function for five particle habits with variables of the effective size and scattering angle. The effective sizes are given by 50, 200 and 400 μm for plate, and 50, 200 and 800 μm for the other four particles. The wavelengths are 0.4, 0.8 and 2.2 μm, respectively. The scattering angles vary from 0° to 180°.

computations for different effective sizes are similar for a specific ice crystal habit. Therefore, the sensitivity of the bidirectional reflectance to particle size at the near-infrared wavelengths is attributed essentially to the dependence of the single-scattering albedo on the particle size. The truncated phase functions for the five ice crystal habits are different. As a result, the bidirectional reflectance is sensitive to particle habit. At a near-infrared wavelength, the single-scattering albedo is also sensitive to particle habit. Therefore, the sensitivity of the bidirectional reflectance for particle habits at an infrared wavelength is attributed to the sensitivity of both the phase function and single-scattering albedo to ice crystal habits.

Acknowledgements

The authors are grateful to Drs. J. F. de Hann, P. B. Bosma, and J. W. Hovenier for using their adding–doubling code, and also to Drs. K. Stammnes, S.-C. Tsay, W. J. Wsicombe, and K. Jayaweera for using their DISORT code. Ping Yang acknowledges the support from the National Science Foundation (ATM-0239605) and the NASA Radiation Sciences Program (NNG04GL24G). George Kattawar acknowledges the support from the Office of Naval Research (N00014-02-1-0478). Michael Mishchenko acknowledges the support from the NASA Radiation Sciences Program and the NASA Glory Mission Project.

References

[1] Wiscombe WJ, Warren SG. A model for the spectral albedo of snow. I: pure snow. J Atmos Sci 1980;37:2712–33.
[2] Dozier J. Spectral signature of alpine snow cover from the Landsat Thematic Mapper. Remote Sens Environ 1989;28:9–22.
[3] Stamnes K, Tsay SC, Wiscombe W, Jayaweera K. Numerically stable algorithm for discrete-ordinate-method radiative transfer in multiple scattering and emitting layered media. Appl Opt 1988;27:2502–9.
[4] Grenfell TC, Warren SG. Reflection of solar radiation by the Antarctic snow surface at ultraviolet, visible, and near-infrared wavelengths. J Geophys Res 1994;D9(18):669–84.
[5] Painter TH, Dozier J. Measurements of the hemispherical–directional reflectance of snow at fine spectral and angular resolution. J Geophys Res 2004;109:D18115.
[6] Kokhanovsky AA, Zege EP. Scattering optics of snow. Appl Opt 2004;43:1589–602.
[7] Kokhanovsky AA, Aoki T, Hachikubo A, Hori M, Zege EP. Reflective properties of natural snow: approximate asymptotic theory versus in situ measurements. IEEE Trans Geosci Remote Sens 2005;43:1529–35.
[8] Mishchenko MI, Dlugach JM, Yanovitskij EG, Zakharova NT. Bidirectional reflectance of flat, optically thick particulate layers: an efficient radiative transfer solution and applications to snow and soil surfaces. JQSRT 1999;63:409–32.
[9] de Hann JF, Bosma PB, Hovenier JW. The adding method for multiple scattering calculations of polarized light. Astron Astrophys 1987;183:371–91.
[10] Wiscombe WJ. The delta-M method: rapid yet accurate radiative flux calculations for strongly asymmetric phase functions. J Atmos Sci 1977;34:1408–22.
[11] Hu YX, Wielicki B, Lin B, Gibson G, Tsay SC, Stamnes K, Wong T. δ-Fit: a fast and accurate treatment of particle scattering phase functions with weighted singular-value decomposition least-squares fitting. JQSRT 2000;65:681–90.
[12] Hapke B. Theory of reflectance and emittance spectroscopy. New York: Cambridge University; 1993.
[13] Chandrasekhar S. Radiative transfer. New York: Dover; 1960.
[14] Mishchenko MI. Vector radiative transfer equation for arbitrarily shaped and arbitrarily oriented particles: a microphysical derivation from statistical electromagnetics. Appl Opt 2002;41:7114–34.
[15] Mishchenko MI. Asymmetry parameters of the phase function for densely packed scattering grains. JQSRT 1994;52:95–110.
[16] Garg R, Prud'homme RK, Aksay IA. Optical transmission in highly concentrated dispersions. J Opt Soc Am A 1998;15:932–5.
[17] Li S, Zhou X. Modeling and measuring the spectral bidirectional reflectance factor of snow-covered sea ice: an intercomparison study. Hydrol Processes 2004;18:3559–81.
[18] Zhang H, Voss KJ. Comparisons of bidirectional reflectance distribution function measurements on prepared particulate surfaces and radiative-transfer models. Appl Opt 2005;44:597–610.
[19] van de Hulst HC. A new look at multiple scattering. New York: Goddard Institute for Space Studies; 1963.
[20] Kattawar GW, Plass GN. Interior radiances in optically deep absorbing media—I. Exact solutions for one-dimensional model. JQSRT 1973;13:1065–80.
[21] Yanovitskij EG. Light scattering in inhomogeneous atmospheres. Berlin: Springer; 1997.
[22] Mishchenko MI, Travis LD, Lacis AA. Multiple scattering of light by particles: radiative transfer and coherent backscattering. Cambridge: Cambridge University Press; 2005.
[23] Yang P, Liou KN. Geometric-optics-integral-equation method for light scattering by nonspherical ice crystals. Appl Opt 1996;35:6568–84.
[24] Auer AH, Veal DL. The dimensions of ice crystals in natural clouds. J Atmos Sci 1970;27:919–26.

[25] Yang P, Liou KN. Single-scattering properties of complex ice crystals in terrestrial atmosphere. Contr Atmos Phys 1998;71:223–48.
[26] Foot JS. Some observation of optical properties of clouds: II. Cirrus. Quart J Roy Meteorol Soc 1988;114:145–64.
[27] Hansen JE, Travis LD. Space Sci Rev 1974;16:527–610.
[28] Takano Y, Liou KN. Solar radiative transfer in cirrus clouds. Part I. Single-scattering and optical properties of hexagonal ice crystals. J Atmos Sci 1989;46:3–19.
[29] Mishchenko MI, Macke A. Incorporation of physical optics effects and δ-function transmission. J Geophys Res 1998;103:1799–805.
[30] Liou KN. An introduction to atmospheric radiation, 2nd ed. San Diego, CA: Academic; 2002.